

A Multi-output Convolutional Neural Network-based Distance and Velocity Estimation Technique

Jae-Woong Choi ¹ and Eui-Rim Jeong ²

¹ Graduate Student, Dept. of Mobile Convergence and Engineering, Hanbat National University, Daejeon, Republic of Korea

²⁺ Professor, Dept. of Information and Communication Engineering, Hanbat National University, Daejeon, Republic of Korea

erjeong@hanbat.ac.kr

Abstract. The objective of this work is to propose a new method of estimating velocity and distance based on multi-output convolutional neural network (CNN) for orthogonal frequency division multiplexing (OFDM) radars. The two-dimensional (2D) periodogram is extracted from the received reflected waveforms through radar signal processing of received OFDM symbols. Conventionally, constant false alarm rate (CFAR) algorithm is used to estimate distance and velocity of targets. In contrast, this paper proposes a novel deep-learning based approach for the estimation of the targets in OFDM radar systems. The proposed multi-output CNN-based target detector estimates the distance and velocity of the target simultaneously. The proposed technique is verified through computer simulation. The results show that the proposed multi-output CNN-based method demonstrates more accurate distance and speed estimates than the conventional CFAR. Specifically, the distance and speed estimates of the proposed method are 9.8 and 12.3 times accurate, respectively, than those of the conventional CFAR.

Keywords: Target estimation, Deep learning, Multi-output CNN, OFDM radar systems, Clutter.

1. Introduction

The radio spectrum is one of the most valuable invisible resource. The demand for

radio spectrum use has been increasing rapidly through mobile wireless terminals such as tablet PCs and smartphone (Na et al., 2018; Singh et al., 2016). Accordingly, the frequency spectrum overcrowding is intensifying due to a surge in data traffic. There is a lot of researches in various fields being conducted to fully utilize insufficient frequency resources (Zhang et al., 2017; Kawamoto et al., 2018). In addition to the spectrum demand for communications, radar systems also require independent frequency resources. In fact, much wider spectrum is needed for radar usage than wireless communications. The utility and importance of radar in many fields as well as future automobiles is expected to explode (Gameiro et al., 2018). To prepare for such a situation in advance, frequency sharing between radar and communication are receiving much interest (Feng et al., 2020). In this field, many researches showed the feasibility for the use of communication waveform such as orthogonal frequency division multiplexing (OFDM) signal as the radar waveform (Barneto et al., 2019).

The OFDM systems are widely used for high-speed wireless communications in 5G and future 6G systems. To cope with the demand for high data rate communications, those OFDM signals uses millimeter waves and over 100 MHz bandwidth. The wideband OFDM waveform satisfies the requirements of high precision radar signals (Shi et al., 2017). Based on the observation, OFDM radar systems have been emerging in research field and the possibility of replacing the existing radar is being considered such as commercial, industrial and military, and automotive fields. The radar techniques for detecting the target's distance and speed using OFDM waveforms have been researched in many literatures. Among them, to the best of the authors' knowledge, convolutional neural network (CNN) based distance and velocity estimators have not been published.

This paper proposes a multi-output CNN-based distance and velocity estimation method for OFDM radar systems. First, the two-dimensional (2D) periodogram is extracted from the received reflected waveforms through radar signal processing. Since this periodogram is two-dimensional signal, it is considered a monochromatic image. This periodogram is input to both the conventional CFAR detector and proposed CNN detector and the detectors estimate distance and velocity of the target. The x-axis of the periodogram indicates velocity and the y-axis indicates distance. The local maximum position of the periodogram represent the reflected objects. Therefore, it is possible to find the distance and velocity of the target by reading the local peaks. Conventional CFAR detector finds the local peaks that exceed a certain threshold. After that, peak values around zero Doppler frequency are regarded as clutters and removed. Thus, only other peaks having non-zero Doppler frequency are left. Since conventional method is based on comparison cell under test (CUT) with threshold, proper threshold is essential to accurately find the peaks. However, the optimal threshold requires the additional information such as noise variance and signal to noise ratio (SNR) which is difficult to acquire in advance. On the other hand,

the proposed multi-output CNN does not require any additional information other than periodogram.

In the proposed method, distance and velocity of the target is estimated through multi-output CNN detector. Usually, typical CNN has one output, but the proposed multi-output CNN has two outputs: one for distance and the other for speed. In other words, conventional CNN has two detectors that estimate the distance and velocity separately but proposed multi-output CNN can estimate two values simultaneously with one CNN. The proposed detector is designed based on ResNet-50 (He et al., 2016). We modify ResNet-50 to estimate the distance and velocity of the target from the periodogram directly. We consider two kinds of CNN inputs: two-dimensional periodogram for the target without clutter components, and two-dimensional periodogram for target with clutter components. The most of radar systems observes for particular targets, but the clutter components mentioned here refer unwanted back-scattered signals or echoes from physical obstacles in the environments such as sea, ground, fixed objects, etc (Chiriyath et al., 2017). Thus, the relative velocity of clutter components is considered zero (O'Connor et al., 2017). In fact, the clutter components always exist. This paper compares the performances under the presence or absence of the clutter components. The simulation is conducted to compare the performance of conventional and proposed methods. The mean absolute error (MAE) was used as a performance indicator, which is averaged difference between the actual value of target and the predicted value. According to the simulation results, as the SNR increases, MAEs decrease. However, the proposed multi-out CNN outperforms the conventional CFAR technique in almost all SNR region in the simulation. At high SNRs, the MAEs of proposed detector are 0.83 m distance MAE and 0.88 km/h speed MAE. Comparing between clutter-presence and clutter-free cases, much more accurate detection is possible when there is no clutter.

2. OFDM radar system model

Figure 1 shows OFDM radar system model considered in this paper. In the signal transmission process, data is modulated and converted from serial to parallel. The m -th generated vector signal is represented as $\mathbf{g}_m = [g_{0,m}, g_{1,m}, \dots, g_{N-1,m}]^T$ where N is FFT length and $g_{n,m}$ is a complex symbol generated through digital modulation. The vector signal \mathbf{g}_m is converted into time domain signal through IFFT. The output of IFFT is denoted by $\mathbf{g}'_m = [g'_{0,m}, g'_{1,m}, \dots, g'_{N-1,m}]^T$. After converting signal from parallel to serial, the guard interval CP which prevents that channel would not leak energy from adjacent OFDM symbol is inserted in front of the signal. The signal inserted CP is denoted by $\mathbf{g}''_m = [g'_{N-L_c,m}, \dots, g'_{N-1,m}, g'_{0,m}, g'_{1,m}, \dots, g'_{N-1,m}]$ where L_c is the length of CP. Then, \mathbf{g}''_m is transmitted via Tx antenna and the reflected signal from the targets is received via Rx antenna. Received signal is denoted as $\mathbf{f}''_m = [f'_{N-L_c,m}, \dots, f'_{N-1,m}, f'_{0,m}, f'_{1,m}, \dots, f'_{N-1,m}]$. \mathbf{g}''_m and \mathbf{f}''_m are not same due to time delay, Doppler frequency and signal attenuation of the

reflected signal. After removing CP of f''_m and converting from serial to parallel, the signal becomes $f'_m = [f'_{0,m}, f'_{1,m}, \dots, f'_{N-1,m}]^T$. Then, by taking FFT the f'_m frequency domain signal is obtained. f_m is defined as the output of FFT and can be written as $f_m = [f_{0,m}, f_{1,m}, \dots, f_{N-1,m}]^T$. It is possible to identify the targets by comparing g_m and f_m . The same procedure is repeated for the neighboring received OFDM symbols and resulting signals are piled up to form a two-dimensional signal.

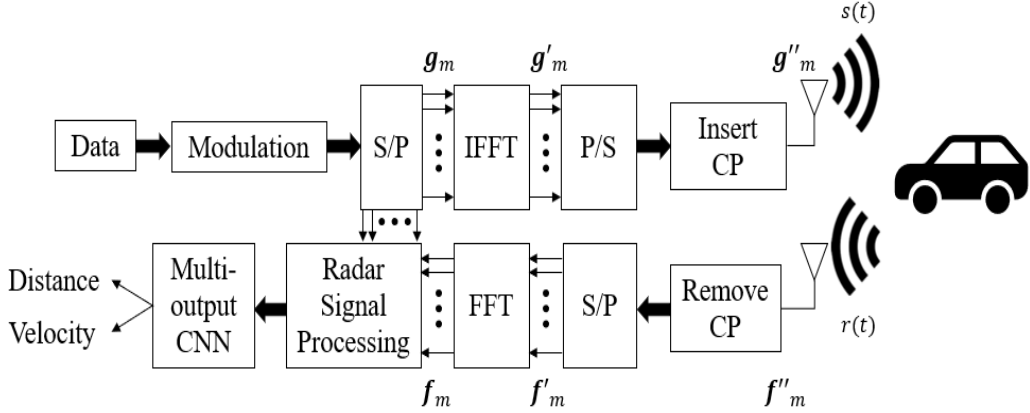


Fig. 1: OFDM radar system model

When the total M OFDM symbols are transmitted, the transmitted matrix and received matrix can be represented as (1) and (2).

$$\mathbf{G} = \begin{pmatrix} g_{0,0} & g_{0,1} & \cdots & g_{0,M-1} \\ g_{1,0} & g_{1,1} & \cdots & g_{1,M-1} \\ \vdots & \vdots & \ddots & \vdots \\ g_{N-1,0} & g_{N-1,1} & \cdots & g_{N-1,M-1} \end{pmatrix} \quad (1)$$

$$\mathbf{F}_r = \begin{pmatrix} f_{0,0} & f_{0,1} & \cdots & f_{0,M-1} \\ f_{1,0} & f_{1,1} & \cdots & f_{1,M-1} \\ \vdots & \vdots & \ddots & \vdots \\ f_{N-1,0} & f_{N-1,1} & \cdots & f_{N-1,M-1} \end{pmatrix} \quad (2)$$

In matrix (1) and (2), each row represents the subcarrier whereas each column represents OFDM symbol index. For instance, $g_{3,7}$ represents the data of 4th subcarrier in 8th OFDM symbol. We assume that the following parameters are known. The sampling frequency after the IFFT is f_s . The subcarrier space is $\Delta f (= f_s/N)$. Accordingly, the OFDM symbol duration is $T (= 1/\Delta f)$. The duration of the CP is T_G . Thus, total duration of OFDM symbol $T_O (= T + T_G)$. The center frequency is f_c .

To perform radar imaging and obtain two-dimensional periodogram, it transmits a signal $s(t)$ and it receives a signal $r(t)$ at the exact same time. The signal $r(t)$ is

composed of a superposition of reflections of the original signal by objects and receiver noise. While transmitting, the receiver receives to pick up the reflected signal. Thus, transmitter and receiver must be synchronized and there should not have any time or frequency offset. The received signal $r(t)$ has the form as

$$r(t) = \sum_{h=0}^{H_t-1} b_h s(t - \tau_h) e^{j2\pi f_{D,h} t} e^{j\phi_h} + \sum_{i=0}^{H_c-1} b_i s(t - \tau_i) e^{j\phi_i} + \tilde{\mathbf{Z}}(t) \quad (3)$$

where H_t is the number of reflecting targets and H_c is the number of clutter components. The time delay causes a phase shift of the individual elements $g_{k,l}$. The phase shift value varies for each subcarrier depending on its frequency. By combining these effects, \mathbf{F}_r is form as

$$(\mathbf{F}_r)_{k,l} = \sum_{h=0}^{H_t-1} b_h (\mathbf{G})_{k,l} e^{j2\pi T o f_{D,h} l} e^{-j2\pi \tau_h \Delta f k} e^{j\phi_h} + \sum_{i=0}^{H_c-1} b_i (\mathbf{G})_{k,l} e^{-j2\pi \tau_i \Delta f k} e^{j\phi_i} + (\tilde{\mathbf{Z}})_{k,l} \quad (4)$$

where $(\mathbf{A})_{k,l}$ indicates the (k, l) -th element of the matrix \mathbf{A} . The time delay is $\tau_h (= 2 \times d_h / c_0)$ which is translated by distance d_h . Doppler frequency is $f_{D,h} (= 2 \times v_{rel,h} / c_0)$ where $v_{rel,h}$ and c_0 are relative velocity and the speed of light, respectively. The ϕ_h is an unknown phase offset and magnitude of the reflected signal b_h is factor of signal attenuation and can be written as

$$b_h = \sqrt{\frac{c_0 \sigma_{RCS,h}}{(4\pi)^3 d_h^4 f_c^2}} \quad (5)$$

where $\sigma_{RCS,h}$, which generally means the size of the target. As mentioned earlier, clutter components refer unwanted back-scattered signals by natural environments or between Tx and Rx antenna. Therefore, equivalent distance and time delays of clutter components are close to zero. The distance of clutter component d_c is generated for simulation by the Weibull distribution of probability density function.

$$f(d_c; \eta, \beta) = \frac{\beta}{\eta} \left(\frac{d_c}{\eta} \right)^{\beta-1} e^{-(d_c/\eta)^\beta} \quad (6)$$

where η and β are scale and shape parameters, respectively. The equivalent radar cross sections are randomly generated with uniform distribution. The matrix $\tilde{\mathbf{Z}} \in \mathcal{C}^{N \times M}$ is Gaussian noise. To remove \mathbf{G} in \mathbf{F}_r , elements-wise division is performed to

yield.

$$\begin{aligned}
 (\mathbf{F})_{k,l} &\triangleq \frac{(\mathbf{F}_r)_{k,l}}{(\mathbf{G})_{k,l}} \\
 &= \sum_{h=0}^{H_t-1} b_h e^{j2\pi T o f_{D,h} l} e^{-j2\pi \tau_h \Delta f k} e^{j\phi_h} + \sum_{i=0}^{H_c-1} b_i e^{-j2\pi \tau_i \Delta f k} e^{j\phi_i} + (\mathbf{Z})_{k,l}
 \end{aligned} \quad (7)$$

where $(\mathbf{Z})_{k,l} = (\tilde{\mathbf{Z}})_{k,l}/(\mathbf{G})_{k,l}$. In (7), first exponential inside the summation contains Doppler frequency and the second exponential contains time delay. The radar problem is to detect and identify two sinusoids. To estimate the sinusoids and sperate for the targets, two-dimensional periodogram is used and has the form as

$$(\mathbf{P})_{N,M} = \frac{1}{NM} \left| \sum_{k=0}^{N-1} \sum_{l=0}^{M-1} (\mathbf{F})_{k,l} (\mathbf{W})_{k,l} e^{-j2\pi \left(\frac{kn}{N_{FFT}} + \frac{lm}{M_{FFT}} \right)} \right|^2 \quad (8)$$

where \mathbf{P} is two-dimensional periodogram and has $N_{FFT} \times M_{FFT}$ size. In (8), The result of the sums inside the modulus operator is called complex periodogram. $N_{FFT} \times M_{FFT}$ is two dimensional DFT (discrete Fourier transform) size. In general, N_{FFT} and M_{FFT} are chosen as integer multiples of N and M to enhance estimation resolution. \mathbf{W} is a window matrix generated by

$$\mathbf{W} = \mathbf{w}_N \mathbf{w}_M^T, \mathbf{w}_N \in R^{N \times 1}, \mathbf{w}_M \in R^{M \times 1} \quad (9)$$

where \mathbf{w}_N and \mathbf{w}_M are one-dimensional window vectors. The Hanning window is used in this paper. If maximum distance and Doppler frequency of targets are limited within certain boundaries, only a cropped region of periodogram \mathbf{P} is sufficient for target detection. Detecting and identifying targets corresponds to the detection of local peaks in the periodogram. If a peak is found at indices (\hat{n}, \hat{m}) , the target distance and relative velocity can be calculated as

$$\hat{d} = \frac{c_0 \hat{n}}{2\Delta f N_{FFT}} \quad (10)$$

$$\hat{v} = \frac{c_0 \hat{m}}{2f_c T M_{FFT}} \quad (11)$$

Owing to the OFDM symbol duration T and the subcarrier spacing Δf , maximum of unambiguous ranges and relative velocities as follows

$$\left| d_{max} \left\| \frac{c_0}{2\Delta f} \right\| \right| \quad (12)$$

$$\left| v_{max} \left\| \frac{c_0}{2f_c T_O} \right\| \right| \quad (13)$$

If Δf and T are designed to be small enough, the maximum unambiguous values can cover the available distance and velocity of targets.

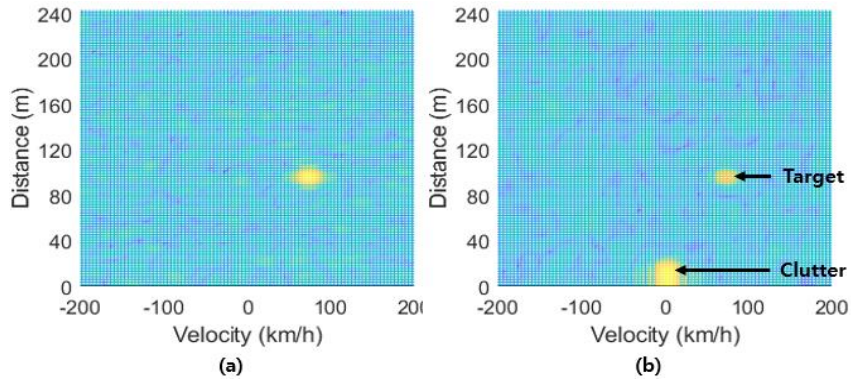


Fig. 2: Example of periodogram, \mathbf{P} , (a) clutter absence (b) clutter presence

The example of \mathbf{P} is shown in Figure 2 when distance and velocity of target are 70 m and 100 km/h, respectively. In Figure 2 (a) shows that the cluster does not exist and (b) shows that clutter components exist. We will call to Figure 2 (a) as clutter absence periodogram and (b) as clutter presence periodogram. The clutter components such as stationary targets are observed where velocity is 0. Positive and negative velocity imply approaching and moving away target, respectively.

3. Estimation technique

The important task of the radar system is detecting the target exactly. In this section, it is described in estimating method the distance and velocity of the target for the conventional method. The conventional CFAR algorithm and multi-output CNN are used for estimation the target.

3.1. Conventional estimation method

Among various CFAR techniques, cell averaging CFAR (CA-CFAR) is most widely used. In CFAR, when the target detection is required for a given cell called as cell under test (CUT), the noise variance is estimated from adjacent cells. Then, the detection threshold, TH , is given by

$$TH = \alpha E_n \quad (14)$$

where E_n is estimated noise power value and α is a threshold factor for scaling threshold. In CFAR technique, a CUT to be tested is and guard cells are defined to be next to the CUT. Training cells (T_i) are established on the outside of guard cells. E_n is estimated from the training cells and can be calculated as

$$E_n = \frac{1}{N_t} \sum_{i=1}^{N_t} T_i \tag{15}$$

where T_i is the sample in each training cell and N_t is the number of training cells.

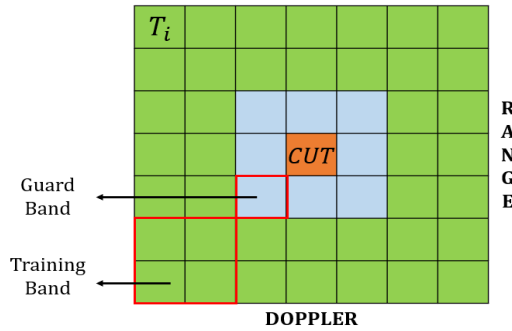


Fig. 3: Example of CFAR detector window

Figure 3 shows an example of 2D CFAR detector window when band (GB) size is 1×1 and the training band (TB) size is 2×2 . Commonly, the number of cells on both sides is the same around CUT. The purpose of guard cells is to avoid signal components from leaking into T_i . The scaling factor α is calculated as

$$\alpha = N_t(P_{fa}^{-1/N_t} - 1) \tag{16}$$

where P_{fa} is the false alarm probability.

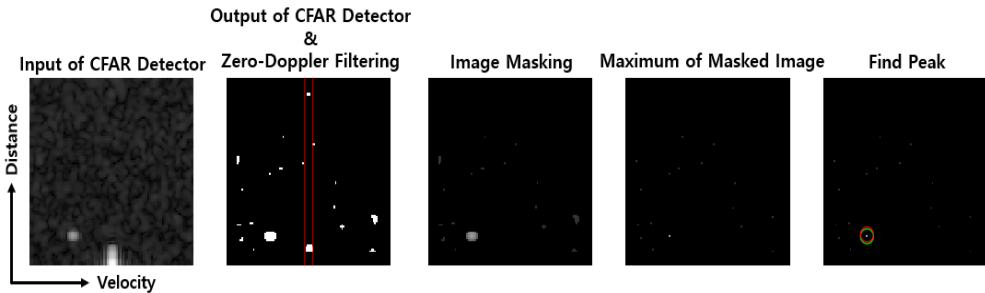


Fig. 4: Process of CA-CFAR detector

Figure 4 shows process of CA-CFAR detector. First, a 2D periodogram is

inputted into the detector and the CFAR detects the targets. The output of CFAR becomes different by the specified TB, GB and P_{fa} . In CFAR algorithm process, noise power is estimated from T_i and the CUT exceeding TH becomes one and otherwise, the CUT becomes zero. Then, clutters are removed by zero Doppler filtering in the CFAR output. The CFAR output is element-wise multiplied by the P . Finally, find the maximum value from the result 2D signal. The maximum is considered as the target. In Figure 4, green circle indicates real coordinate and red circle indicates predicted coordinate. In zero-Doppler filtering procedure, the target with relative velocity close to zero can be discarded. This cause detection error and may be a potential problem of CFAR.

3.2. Proposed estimation method

The proposed multi-output CNN detector predicts the distance and velocity of the target from the periodogram. The CNN is one of the deep learning techniques, specialized in image classification (Wang et al., 2016; Jeong et al., 2020; Nam & Jeong, 2020). Finding peaks in periodogram can be regarded as an image detection problem. Therefore, it is suitable for solving radar problems using CNN. Usually, a typical CNN has one output, but the proposed multi-output CNN has two outputs. When using a typical CNN, there should be at least two detectors that estimate distance and velocity, respectively. However, proposed multi-output CNN can estimate at once with just one detector. The proposed multi-output CNN structure is as shown in Figure 5. The model is based on ResNet-50 but has different input and outputs size. The input layer, convolutional layers and the each fully connected layer are linked, and at the end, each of two different fully connected layers (fc) receives the last pooling layer's output. Finally, the value corresponding to the distance and velocity is predicted. As mentioned earlier, there are two cases of input. One is for clutter absence image, the other is for clutter presence image. The input signal is cropped periodogram that size is $S \times S$. The number of the fully connected layer output is 1 for regression. The input or output size of CNN are varied by number of OFDM symbols, 2D FFT size and available target detection range. The proposed CNN detector only requires periodogram signal. Unlike the proposed method, CFAR require additional information such as noise power estimate and noise variance.

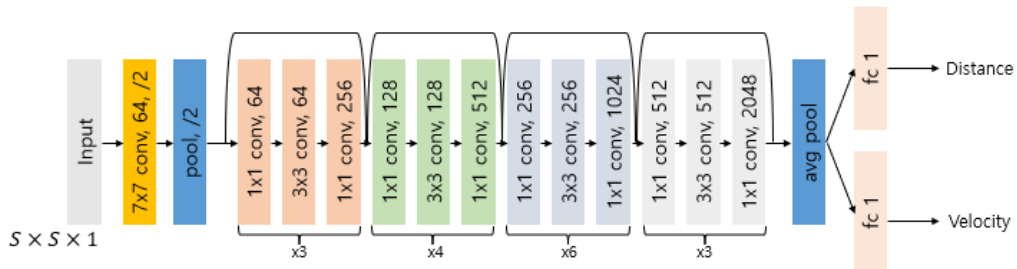


Fig. 5: Proposed multi-output CNN structure

4. Results

4.1. Simulation environment

The periodogram is generated and performance of conventional CFAR detector were verified through Matlab. The performance of the proposed multi-output CNN was demonstrated through computer simulation using Tensorflow. In the simulation, $f_s = 122.88\text{MHz}$, $N = 4096$, $M = 16, 32, 64, 128$, $N_{FFT} = 2048$, $M_{FFT} = 128$ and L_c is 296. Thus, the symbol duration is $T_o = 35.74\mu\text{s}$. The subcarrier spacing is $\Delta f = 30\text{kHz}$. Among total 4,096 subcarriers, only 1,284 subcarriers are used, and the resulting signal bandwidth is about 40MHz . The carrier frequency is $f_c = 28\text{GHz}$. For training dataset, the reflected signals on a target are randomly generated from SNR -14 dB to +22 dB. We crop the periodogram by 100×100 . Due to the cropped 2D periodogram, the detectable range of distance and velocity is from 7 m to 230 m and from -190 km/h and 190 km/h, respectively. The clutter components are randomly generated using Weibull distribution and the associated parameters are $\eta = 1$ and $\beta = 1$. In the conventional method, the parameters GB sizes and TB are 1×1 and 5×5 , respectively. Also, P_{fa} for 16, 32 and 64 symbols are 0.24, 0.21 and 0.21, respectively. Figure 6 shows the spectrum of generated OFDM signals when $M = 64$.

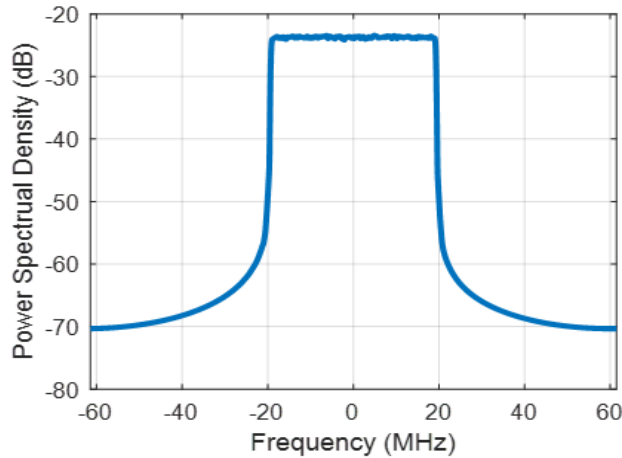


Fig. 6: Spectrum of OFDM signal

4.2. Training multi-output CNN

The proposed multi-output CNN learns from the periodograms and corresponding distance and velocity labels. As mentioned earlier, there are two case of input signal \mathbf{P} : clutter free and clutter presence periodograms. The number of training data N_d used is 110,000 and the mini-batch size is 100. The maximum epoch is 200 for clutter absence case and 800 for clutter presence case. Therefore, the parameters update 1,100 times in each epoch and total number of parameter updates is 220,000 and 880,000, respectively. The optimization algorithm is Adam with learning rate 0.001. Both clutter absence and clutter presence periodogram has 100×100 input size and

the number of trainable parameters is 23,536,516. The loss function is mean square error (MSE) and can be written as

$$MSE = \frac{1}{N_d} \sum_{i=1}^{N_d} (\hat{d}_i - d_i)^2 + (\hat{v}_i - v_i)^2 \quad (17)$$

In (17), N_d is the number of training data, \hat{d}_i and \hat{v}_i are the distance and velocity output of the CNN during the learning process, respectively. The d_i and v_i are actual distance or velocity values of target.

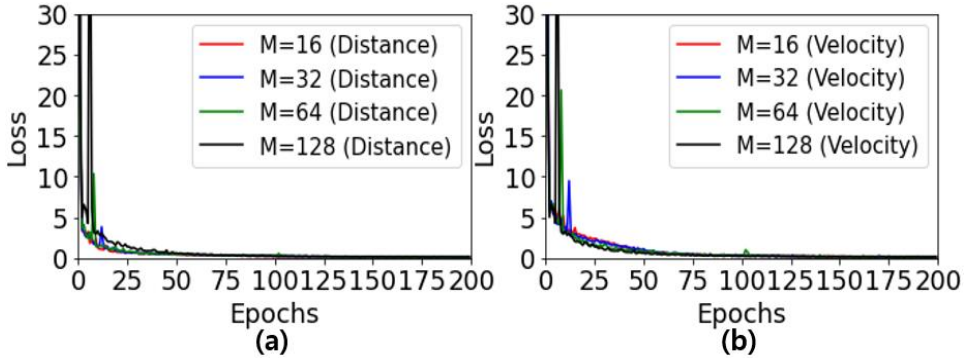


Fig. 7: Learning Curves for Clutter Absence Periodogram,
(a) Distance MSE (b) Velocity MSE

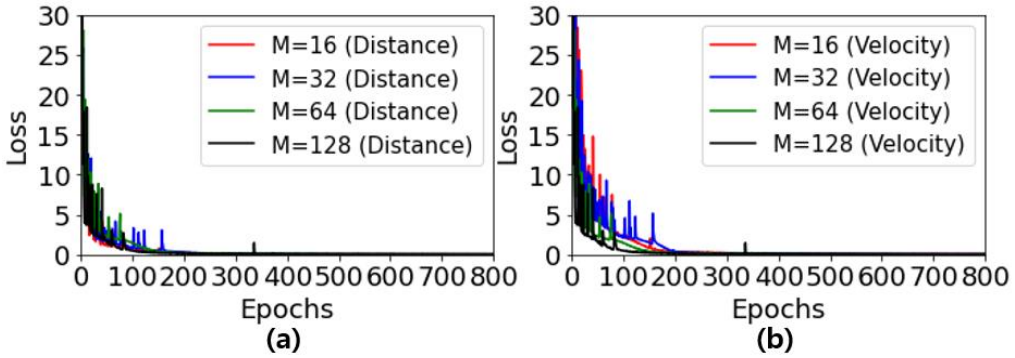


Fig. 8: Learning Curves for Clutter Presence Periodogram,
(a) Distance MSE (b) Velocity MSE

Figures 7 and 8 show the learning curves for clutter absence periodogram and clutter presence periodogram, respectively. The number of the targets, H_t is 1 and the number of clutter components H_c is 0 for (a) and 20 for (b). As shown in the Figures, the losses gradually decrease and finally converges to zeros. In the early stage of learning, losses have not stabilized, but convergence is observed as training iteration increases.

4.3. Performance comparison

For performance verification of the proposed technique, new test signals are generated. Each periodogram for the test, the distance d_h and velocity $v_{rel,h}$ of targets is also generated randomly but the SNRs of the targets are the same. The SNR ranges from -20 dB to +22 dB with 3 dB step. 10,000 test periodograms are generated at each SNR. The performance of the CFAR detector and the proposed multi-output CNN is compared using test periodogram. MAE is used as a performance indicator. The MAE can be written as

$$MAE = \frac{1}{N_e} \sum_{n=1}^{N_e} |\hat{y}_n - y_n| \quad (18)$$

where N_e is the number of test data, \hat{y}_n is output of multi-output CNN that is predicted value and y_n is actual value of target.

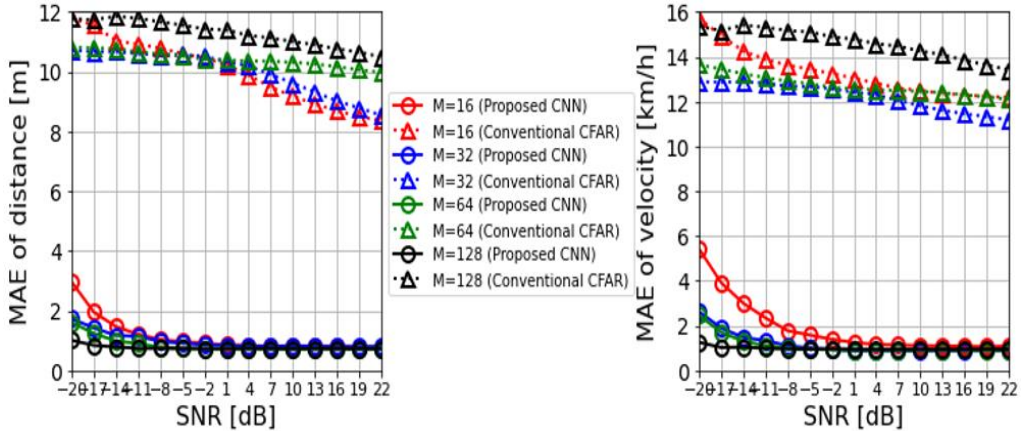


Fig. 9: MAE performance for conventional and proposed method, clutter presence case only
 (a) MAE of distance (b) MAE of velocity

Figure 9 (a) shows MAEs of distance and (b) shows MAEs of velocity for conventional CFAR and proposed multi-output CNN in clutter presence environment. As the SNR increases, all MAEs improves. In Figure 9, in case of CFAR, distance MAE is 8.2 m and velocity MAE is 10.8 km/h at best throughout all symbols. On the other hand, proposed CNN has the best performance when SNR is 22 dB and $M = 128$, and the distance and velocity MAEs are 0.83 m and 0.88 km/h, respectively. The differences in MAEs between conventional and proposed method are about 7.37 m and 9.92 km/h. The proposed technique shows much accurate distance and speed estimation.

Figure 10 shows MAE performance comparison of proposed CNN between clutter presence and clutter free cases. Figure 10 (a) is the performance when clutter is presence and (b) is absence. In both (a) and (b), as the SNR increases, all MAEs

decrease. In addition, as the number of transmitted symbols increases, the performance in the lower SNR range also improves. The performance of clutter absence case is superior to presence case when same symbols are transmitted. At $M = 128$ and SNR 22 dB, the difference of distance MAE is about 0.56 m and velocity MAE is about 0.61 km/h.

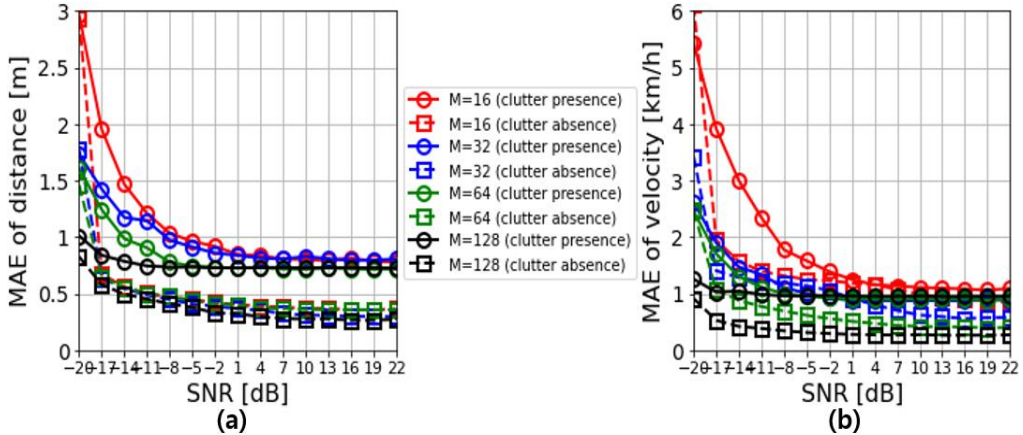


Fig. 10: MAE performance for proposed method only, clutter absence and presence cases
(a) MAE of distance (b) MAE of velocity

In other words, the proposed estimates of distance and speed are 9.8 and 12.3 times more accurate than the conventional CFAR. When comparing the proposed techniques with and without clutters, the MAEs of distance and speed estimates without clutters are 3.1 and 3.3 times lower, respectively, than those with clutters. Those results indicate that clutter components increase misdetection of the targets due to confusion between the target and the clutter. In clutter presence case, however, properly increasing the number of the transmission symbols M can decrease error in estimating distance and velocity.

5. Conclusion

This paper proposed a new target detection technique for OFDM radar systems. The proposed detector was developed based on 2D multi-output CNN techniques. By taking the 2D periodogram of the reflected OFDM signals as the CNN input, the 2D CNN directly estimates the distance and the velocity of the target without any additional information. Through computer simulation, the proposed technique was compared with the most famous conventional CFAR technique. According to the computer simulation results, the proposed technique outperforms the conventional CFAR. Specifically, the MAEs of distance and speed are 9.8 and 12.3 times lower, respectively. Those results indicates that the proposed technique estimates the target's distance and velocity much more accurately. If the proposed technique is employed in 5G or 6G mobile communications, real-time beamforming and beam-tracking can

be realized by performing radar signal processing while communicating between the base station and the mobile station. If that happens, the proposed technique may be a revolutionary turning point for high-speed communication in millimeter-wave mobile environments.

Acknowledgements

This work was supported by Institute of Information & communications Technology Planning & Evaluation (IITP) grant funded by the Korea government (MSIT) (No.2018-0-01663, Development of Communication-Sensing Converged B5G Millimeter Wave System)

References

- Barneto, C. B., Riihonen, T., Turunen, M., Anttila, L., Fleischer, M., Stadius, K., Ryyänen, J. & Valkama, M. (2019). Full-duplex OFDM radar with LTE and 5G NR waveforms: Challenges, solutions, and measurements. *IEEE Transactions on Microwave Theory and Techniques*, 67(10), 4042-4054.
- Chiriyath, A. R., Paul, B., & Bliss, D. W. (2017). Simultaneous radar detection and communications performance with clutter mitigation. In *2017 IEEE Radar Conference (RadarConf)* (pp. 0279-0284).
- Feng, Z., Fang, Z., Wei, Z., Chen, X., Quan, Z., & Ji, D. (2020). Joint radar and communication: A survey. *China Communications*, 17(1), 1-27.
- Gameiro, A., Castanheira, D., Sanson, J., & Monteiro, P. P. (2018). Research challenges, trends and applications for future joint radar communications systems. *Wireless Personal Communications*, 100(1), 81-96.
- He, K., Zhang, X., Ren, S., & Sun, J. (2016). Deep residual learning for image recognition. In *Proceedings of the IEEE conference on computer vision and pattern recognition* (pp. 770-778).
- Jeong, E. R., Lee, E. S., Joung, J., & Oh, H. (2020). Convolutional neural network (CNN)-based frame synchronization method. *Applied Sciences*, 10(20), 7267.
- Kawamoto, Y., Takagi, H., Nishiyama, H., & Kato, N. (2018). Efficient resource allocation utilizing Q-learning in multiple UA communications. *IEEE Transactions on Network Science and Engineering*, 6(3), 293-302.
- Na, W., Jang, S., Lee, Y., Park, L., Dao, N. N., & Cho, S. (2018). Frequency resource allocation and interference management in mobile edge computing for an Internet of Things system. *IEEE Internet of Things Journal*, 6(3), 4910-4920.

Nam, G. M., & Jeong, E. R. (2020). Distance Estimation Based on Deep Convolutional Neural Network Using Ultra-Wideband Signals. *Journal of Computational and Theoretical Nanoscience*, 17(7), 3212-3217.

O'Connor, A. C., Kantor, J. M., & Jakabosky, J. (2017). Filters that mitigate waveform modulation of radar clutter. *IET Radar, Sonar & Navigation*, 11(8), 1188-1195.

Shi, C., Wang, F., Sellathurai, M., Zhou, J., & Salous, S. (2017). Power minimization-based robust OFDM radar waveform design for radar and communication systems in coexistence. *IEEE Transactions on Signal Processing*, 66(5), 1316-1330.

Singh, V., Lentz, M., Bhattacharjee, B., La, R. J., & Shayman, M. A. (2016). Dynamic frequency resource allocation in heterogeneous cellular networks. *IEEE Transactions on Mobile Computing*, 15(11), 2735-2748.

Wang, J., Yang, Y., Mao, J., Huang, Z., Huang, C., & Xu, W. (2016). Cnn-rnn: A unified framework for multi-label image classification. In *Proceedings of the IEEE conference on computer vision and pattern recognition* (pp. 2285-2294).

Zhang, J., Tang, P., Tian, L., Hu, Z., Wang, T., & Wang, H. (2017). 6–100 GHz research progress and challenges from a channel perspective for fifth generation (5G) and future wireless communication. *Science China Information Sciences*, 60(8), 1-18.